Autonomous Synchronization of Satellite Constellations via Optical Inter-Satellite Links

Christian Trainotti, Manuele Dassié, Gabriele Giorgi
Institute of Communications and Navigation
German Aerospace Center (DLR)
Weßling, Germany
christian.trainotti@dlr.de

Amir Khodabandeh
Department of Infrastructure Engineering
University of Melbourne
Melbourne, Australia

Christoph Günther
Institute of Communications and Navigation
German Aerospace Center (DLR)
Weßling, Germany
and
Institute of Communications and Navigation
Technical University of Munich
Munich, Germany

***Abstract*—In this paper we present an on-board clock steering scheme for achieving tight synchronization of constellations interconnected with optical inter-satellite links. Thanks to the links, a distributed space-based clock ensemble can be formed, with a clock steering system on each satellite providing a physical local realization of the system time. An analytical method for determining the synchronization performance is derived.**

Keywords—optical inter-satellite links, GNSS, timescale, clock ensemble, synchronization.

I. Introduction

Global navigation satellite systems (GNSSs) of the next generation are going to take advantage of inter-satellite links (ISLs), connecting satellites across the constellation and providing improved services and robustness. The ISLs provide pseudorange measurements, clock offset observations, integrity monitoring, as well as data communication between satellites, resulting in a number of cascading benefits. Radio-frequency ISLs are already in use e.g. in the BeiDou system and are planned in Galileo second generation [1]. On the other hand, optical links have reached technological maturity and have been applied for communication for a number of years in the European Data Relay System (EDRS). Additionally, [2] showed that a proper modulation of the optical carrier can enable time-transfer and ranging capabilities with a precision at millimeter level for pseudorange measurements and picosecond level for time transfer. Taking advantage of these capabilities, the use of optical intersatellite link (OISLs) in future GNSS systems brings a variety of benefits.

In current systems, the free-running clocks of the satellites are co-estimated in complex orbit determination and time synchronization (ODTS) processing schemes. In the ground segment, the system time scale is defined by a composite clock (GPS) or by using a master clock (Galileo). The offset of each satellite's clock to system time is determined in post-processing, from which clock corrections are computed and predicted for a few hours. The user applies these corrections to account for the offset of the satellites' clocks to the system time. Nowadays this process is accurate to nanosecond-level.

Thanks to the time-transfer accuracy enabled by bidirectional OISLs, future systems, such as the Kepler design proposed by DLR [3], can adopt an onboard real-time synchronization: the satellites directly compute system time, and accordingly correct their onboard clocks. This results in a constellation of synchronized signals, transmitting the navigation messages in a highly synchronized manner. Such a synchronization scheme removes the need to compute and broadcast single clock corrections, so that a ground-based support for clock synchronization is not required.

In this paper, we describe the satellite synchronization scheme based on OISLs. The nominal performance is estimated by using recursive computations of key system parameters and compared to Monte-Carlo simulations. The effect of unmodelled measurement biases on the synchronization performance is discussed. Finally, a simulation shows how an open ring configuration, compared to a closed ring, affects the achievable performance.

II. Distributed clock ensemble

Via the OISLs, each satellite can retrieve the time offsets between the onboard timescale and the timescales realized by the neighboring satellites [3]. The differential measurements between satellites are continuously relayed across the constellation with small latency. In this way, all differential measurements are available on every satellite, so that all satellites can execute a clock ensembling algorithm based on identical measurements. The clock ensemble, comprising all

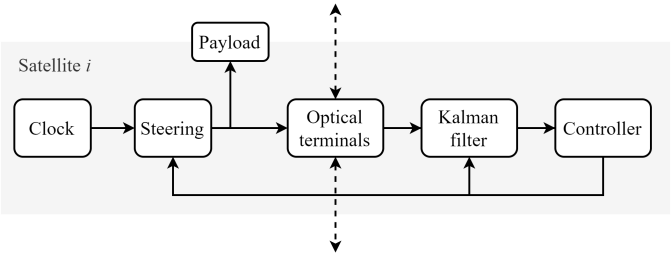

Fig. 1. Scheme of the timing system on board a satellite. The signal of a steered oscillator drives the payload and the optical terminals. These establish optical inter-satellite links to the neighboring satellites. The measurements are fed to a Kalman filter, whose output is used by a controller to compute the steering action.

clocks in the constellation, can be generated on board, and by steering the local clock towards to the composite time scale, each satellite can realize a local copy of the composite time scale. This results in tightly synchronized satellites.

A simplified scheme of the synchronization system on board a satellite is depicted in Fig. 1: the signal of the local clock is steered by a steering device, which applies frequency steps according to the inputs from a controller. The output of the steering device is the signal synchronized to system time, used by the payload and by the optical terminals. The payload in GNSS constellations is the radiofrequency signal generator. The optical terminals establish OISLs to the neighboring satellites and provide the differential measurements between clocks. A Kalman filter uses this data to estimate the state of the ensemble clocks according to a predefined model. Finally, the estimated state is used by the controller to keep the local clock synchronized to the composite time scale.

A. Clock model

The model of the ensemble comprises the single models of the constellation clocks and a model of the measurements between satellites:

$$\mathbf{x}_{k+1} = \mathbf{\Phi}\mathbf{x}_k + \mathbf{B}\mathbf{u}_k + \mathbf{w}_k \ , \tag{1}$$

$$\mathbf{z}_{k+1} = \mathbf{H}\mathbf{x}_{k+1} + \mathbf{v}_{k+1}, \tag{2}$$

where $\mathbf{x}$ is the state vector containing the phase and frequency of each clock and the states of Gauss-Markov processes, if needed to model additional noise components characterizing the clocks [4]; $\mathbf{\Phi}$ is the state propagation matrix; the matrix $\mathbf{B}$ propagates the steering action $\mathbf{u}$; $\mathbf{z}$ is the vector of differential clock measurements computed with the measurement matrix $\mathbf{H}$; $\mathbf{w} \sim \mathcal{N}(0, \mathbf{Q})$ and $\mathbf{v} \sim \mathcal{N}(0, \mathbf{R})$ represent the process noise and the measurement noise, respectively. The subscript k indicates the k-th time step. All matrices in (1) are computed from clock noise parameters depending on the types of clocks on the satellites [4]. The measurement matrix and the covariance matrix in (2) are computed according to the topology of OISLs and their measurement noise level. For instance, supposing an ensemble with 3 clocks, with phase difference measurements taken in a ring configuration (2-1, 3-2, 1-3) and 2 states per clock, the measurement matrix would be

$$\mathbf{H} = \begin{bmatrix} -1 & 0 & 1 & 0 & 0 & 0 \\ 0 & 0 & -1 & 0 & 1 & 0 \\ 1 & 0 & 0 & 0 & -1 & 0 \end{bmatrix} . \tag{3}$$

B. Kalman filter

The Kalman filter estimates the clocks' real states in three steps [5], [6]:
Time update:

$$\mathbf{x}_k^- = \mathbf{\Phi}\mathbf{x}_{k-1}^+ + \mathbf{B}\mathbf{u}_{k-1} \tag{4a}$$

$$\mathbf{P}_k^- = \mathbf{\Phi}\mathbf{P}_{k-1}^+\mathbf{\Phi}^\top + \mathbf{Q} \tag{4b}$$

Kalman gain computation:

$$\mathbf{K}_k = \mathbf{P}_k^-\mathbf{H}^\top \left(\mathbf{H}\mathbf{P}_k^-\mathbf{H}^\top + \mathbf{R}\right)^{-1} \tag{5}$$

Measurement update:

$$\mathbf{x}_k^+ = \mathbf{x}_k^- + \mathbf{K}_k \left(\mathbf{z}_k - \mathbf{H}\mathbf{x}_k^-\right) \tag{6a}$$

$$\mathbf{P}_k^+ = \left(\mathbf{I} - \mathbf{K}_k\mathbf{H}\right)\mathbf{P}_k^- \tag{6b}$$

where $\mathbf{x}^-$ is the predicted state estimate, $\mathbf{P}^-$ the covariance of the predicted estimation error, $\mathbf{K}$ the Kalman gain, $\mathbf{x}^+$ the corrected state estimate, and $\mathbf{P}^+$ the covariance of the corrected estimation error. The additional step of covariance reduction removes the unbounded growth of the covariance matrix due to system unobservability using the reduction matrix $\mathbf{S}_k$

$$\mathbf{P}_k^+ \leftarrow \mathbf{S}_k\mathbf{P}_k^+\mathbf{S}_k^\top \ . \tag{7}$$

The reduced covariance matrix $\mathbf{P}_k^+$ is then used in the following iteration of the Kalman filter. The reduction matrix $\mathbf{S}_k$ is computed at every step from the corrected covariance matrix $\mathbf{P}_k^+$ before reduction, as in [5]:

$$\mathbf{S}_k = \mathbf{I}, \quad \mathbf{S}_{\mathrm{xx},k} = \mathbf{I} - \mathbf{1}\mathbf{a}_k^\top \ , \tag{8}$$

where $\mathbf{S}_{\mathrm{xx},k}$ selects the submatrix of $\mathbf{S}_k$ corresponding to the phase states of all the clocks, $\mathbf{1}$ is a column vector of ones, and $\mathbf{a}_k$ are the clock weights

$$\mathbf{a}_k = \frac{\left(\mathbf{P}_{\mathrm{xx},k}^+\right)^{-1}\mathbf{1}}{\mathbf{1}^\top\left(\mathbf{P}_{\mathrm{xx},k}^+\right)^{-1}\mathbf{1}} \ , \tag{9}$$

with $\mathbf{P}_{\mathrm{xx},k}^+$ selecting the submatrix of $\mathbf{P}_k^+$ corresponding to the phase states of all the clocks.

C. Implicit ensemble mean and steering

The clocks can be corrected using the estimates of the clocks' states provided by the Kalman filter. This yields the (unobservable) *corrected clocks* $\tilde{\mathbf{x}}^+ = \mathbf{x}_k - \mathbf{x}_k^+$, which are Gaussian distributed with covariance matrix $\mathbf{P}^+$. The average of the corrected clocks, weighted according to $\mathbf{P}^+$, is the so-called implicit ensemble mean (IEM) [5], [7]. Its value can only be computed in simulation, because the real clocks states $\mathbf{x}_k$ are not accessible in a real scenario. Although the corrected clocks are unobservable, it is possible to steer the clocks by

using the Kalman filter estimates. Thus, at steady-state each steered clock approximates the respective corrected clock.

The controller computes the steering action to be applied to each steered clock as

$$\mathbf{u}_k = -\mathbf{G}\mathbf{x}_k^+ \ , \tag{10}$$

where $\mathbf{G}$ is the steering gain matrix, not to be confused with the Kalman gain $\mathbf{K}$. The steering gain $\mathbf{G}$ can be computed using different methods, such as the pole placement or the linear-quadratic regulator [8].

III. Performance evaluation

The goal of the study is to verify the synchronization achievable with varying precision and accuracy of the OISLs. We define the desynchronization as the difference between any two steered clocks in the constellation:

$$\boldsymbol{\delta}_k = \boldsymbol{\Delta}\mathbf{x}_k \ , \tag{11}$$

where $\boldsymbol{\Delta}$ is a matrix taking all the permutations between the phases of any two clocks. The desynchronization $\boldsymbol{\delta}_k$ is a stochastic quantity, depending on the time instant t_k, whose mean and covariance stabilize to constant values after an initial transient phase.

To evaluate a worst-case scenario, we want to determine the maximum desynchronization between satellites in the system, thus the steady-state mean and variance of the desynchronization must be evaluated. Analyzing the system closed-loop transfer function is not trivial, due to the system's unobservability, the additional step of covariance reduction, and the stochastic diffusive noise processes in the system. Thus, in this paper we develop several recursive expressions to evaluate the steady-state values of key quantities of the system starting from defined initial values. These results are validated via Monte-Carlo simulations.

A. Nominal performance

By following the approach in [9], we rewrite the state vector as

$$\mathbf{x}_k = \tilde{\mathbf{x}}_k^- + \mathbf{x}_k^- \ , \tag{12}$$

where $\tilde{\mathbf{x}}^-$ is the predicted estimation error and $\mathbf{x}^-$ the predicted state estimate. Assuming uncorrelated process and measurement noises, state estimate $\mathbf{x}^-$ and estimation error $\tilde{\mathbf{x}}^-$ also result uncorrelated. Thus, we compute the mean-square value (MSV) as

$$\boldsymbol{\Sigma}_k = \mathbf{E}\left(\mathbf{x}_k\mathbf{x}_k^\top\right) = \mathbf{P}_k^- + \boldsymbol{\Sigma}_k^- \ , \tag{13}$$

where $\boldsymbol{\Sigma}_k^-$ is the MSV of $\mathbf{x}_\mathbf{k}^-$. $\boldsymbol{\Sigma}_k^-$ can be found from the dynamics equation for the a-priori estimate:

$$\mathbf{x}_{k+1}^- = (\boldsymbol{\Phi} - \mathbf{BG})\left(\mathbf{x}_k^- + \mathbf{K}_k\mathbf{H}\tilde{\mathbf{x}}_k^- + \mathbf{K}_k\mathbf{v}_k\right) \ , \tag{14}$$

from which

$$\boldsymbol{\Sigma}_{k+1}^- = (\boldsymbol{\Phi} - \mathbf{BG})\left(\boldsymbol{\Sigma}_k^- + \mathbf{K}_k\left(\mathbf{H}\mathbf{P}_k^-\mathbf{H}^\top + \mathbf{R}\right)\mathbf{K}_k^\top\right)(\boldsymbol{\Phi} - \mathbf{BG})^\top \ , \tag{15}$$

since the predicted state vector $\mathbf{x}_k^-$ and the measurement noise $\mathbf{v}_k$ are uncorrelated. The recursion can be initialized with

$$\boldsymbol{\Sigma}_0^- = (\boldsymbol{\Phi} - \mathbf{BG})\left(\mathbf{x}_0\mathbf{x}_0^\top\right)(\boldsymbol{\Phi} - \mathbf{BG})^\top \ . \tag{16}$$

Please note that only if no covariance reduction is performed, (15) can be reduced to

$$\boldsymbol{\Sigma}_{k+1}^- = (\boldsymbol{\Phi} - \mathbf{BG})\left(\boldsymbol{\Sigma}_k^- + \mathbf{P}_k^- - \mathbf{P}_k^+\right)(\boldsymbol{\Phi} - \mathbf{BG})^\top . \tag{17}$$

The expected value of the clocks can be found by observing that the steered clocks reach the corrected clocks at steady-state. We define $\boldsymbol{\omega}_{k+1} = \mathbf{E}\left(\tilde{\mathbf{x}}_{k+1}^+\right)$ and thus

$$\boldsymbol{\omega}_{k+1} = (\mathbf{I} - \mathbf{K}_{k+1}\mathbf{H})\,\boldsymbol{\Phi}\boldsymbol{\omega}_k \tag{18}$$

which can be derived from the estimation error dynamic equation

$$\tilde{\mathbf{x}}_{k+1}^+ = (\mathbf{I} - \mathbf{K}_{k+1}\mathbf{H})\,\boldsymbol{\Phi}\tilde{\mathbf{x}}_k^+ + (\mathbf{I} - \mathbf{K}_{k+1}\mathbf{H})\,\mathbf{w}_k - \mathbf{K}_{k+1}\mathbf{v}_{k+1} \ . \tag{19}$$

The recursion can be initialized with

$$\boldsymbol{\omega}_0 = \mathbf{x}_0 - \mathbf{x}_0^- \ . \tag{20}$$

Thus, we have

$$\mathbf{x}_k \sim \mathcal{N}\left(\boldsymbol{\omega}_k, \boldsymbol{\Sigma}_k\right), \ \boldsymbol{\delta}_k \sim \mathcal{N}\left(\boldsymbol{\Delta}\boldsymbol{\omega}_k, \boldsymbol{\Delta}\boldsymbol{\Sigma}_k\boldsymbol{\Delta}^\top\right). \tag{21}$$

The initialization of the recursions (16) and (20) require knowing the initial state vector $\mathbf{x}_0$, which is unobservable in a real case. Setting a wrong initial value does not influence the steady-state value of $\boldsymbol{\Sigma}^-$, while it causes a shift in $\boldsymbol{\omega}$. While the expected value of the steered clocks is influenced, their difference is unaffected, so that the resulting desynchronization $\boldsymbol{\delta}$ does not depend on the initial value $\mathbf{x}_0$. Furthermore, the analyses shown here are meant for an offline evaluation of different constellation designs, but are not influencing the real-time onboard synchronization algorithm.

By means of 2000 Monte-Carlo simulations, the distribution can be verified after a settling time of 200 seconds for an ensemble of 3 clocks with (q_x, q_y) [5] noise parameters (2.16, 2.86e-4), (8.6e-2, 7.1e-3), and (2.4e-3, 7.1e-3). The clocks are measured in a ring configuration (2-1, 3-2, 1-3) with measurement noise covariance 0.1. The steering is executed every second, the gain matrix is computed using the pole-placement method with parameter $\lambda = 0.6$.

Fig. 2 shows the resulting distributions of the phases of the 3 clocks, Fig. 3 shows the distributions of the desynchronization. The theoretical distribution (solid lines) are in agreement with the observed distributions from Monte-Carlo simulations. Furthermore, we can observe that some pairs of clocks are characterized by a desynchronization with higher variance, caused by the higher short term noise of the clocks being compared.

B. Non-nominal performance: constant measurement biases

In this section we modify the analysis of the nominal performance to account for unmodelled measurement biases. The rationale behind this is the possibility that the optical terminals and the onboard electronics cause hardware delays

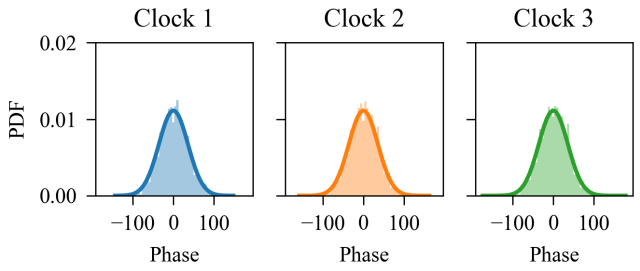

Fig. 2. Distribution of the phases of 3 steered clocks (arbitrary units). The theoretical distributions (solid lines) agree with the Monte-Carlo simulations.

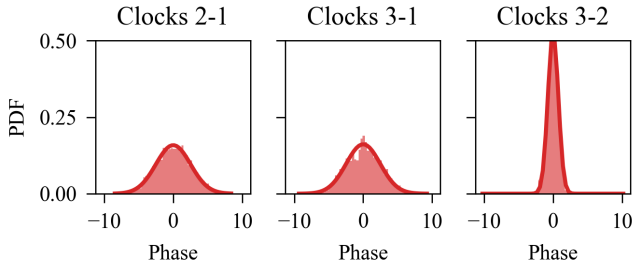

Fig. 3. Distribution of the differences between the 3 steered clocks (arbitrary units). The theoretical distributions (solid lines) agree with the Monte-Carlo simulations.

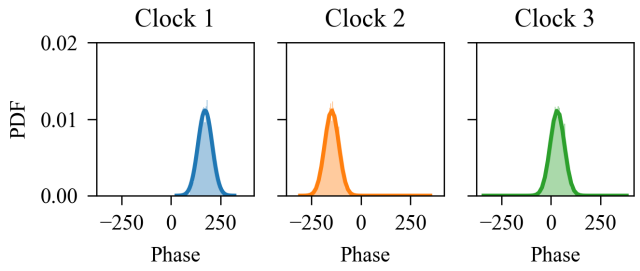

Fig. 4. Distribution of the phases of 3 steered clocks (arbitrary units) with measurement bias. The theoretical distributions (solid lines) agree with the Monte-Carlo simulations.

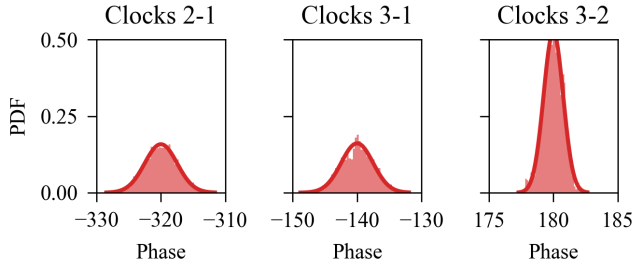

Fig. 5. Distribution of the differences between the 3 steered clocks (arbitrary units) with measurement bias. The theoretical distributions (solid lines) agree with the Monte-Carlo simulations. Note the different scaling of the x-axes.

in the measurements between clocks. These delays can be calibrated and corrected, but not completely eliminated. Thus, it is important to

1) evaluate the impact of the residual hardware delays on the system and on the synchronization level;
2) evaluate how precisely the hardware delays must be calibrated.

Equation (2) is modified and a bias vector $\mathbf{b}$ added to the measurement:

$$\mathbf{z}_k = \mathbf{H}\mathbf{x}_k + \mathbf{b} + \mathbf{v}_k \ . \tag{22}$$

In this paper we consider the bias vector to be constant in time. The Kalman filter estimates the clock states without knowledge of the added bias, thus introducing an estimation error. Since the bias only affects the observations of the system, all matrices of the filter, as well as the MSV obtained in section III-A, are unchanged. However, the estimation error dynamics equation contains a new term. Thus, (19) and (18) respectively become

$$\tilde{\mathbf{x}}^+_{k+1} = (\mathbf{I} - \mathbf{K}_{k+1}\mathbf{H})\,\mathbf{\Phi}\tilde{\mathbf{x}}^+_k + (\mathbf{I} - \mathbf{K}_{k+1}\mathbf{H})\,\mathbf{w}_k - \mathbf{K}_{k+1}(\mathbf{b} + \mathbf{v}_{k+1}) \tag{23}$$

and

$$\boldsymbol{\omega}_{k+1} = \mathbf{E}\left(\tilde{\mathbf{x}}^+_{k+1}\right) = (\mathbf{I} - \mathbf{K}_{k+1}\mathbf{H})\,\mathbf{\Phi}\boldsymbol{\omega}_k - \mathbf{K}_{k+1}\mathbf{b}. \tag{24}$$

Therefore, the measurement bias does not affect the distribution of the clocks' estimates, but rather the corrected clocks. This leads to an increase in desynchronization between the steered clocks. For verification purposes, a bias is injected in the ensemble described in section III-A:

$$\mathbf{b} = [b_{2-1}, b_{3-2}, b_{1-3}]^\top = [300, -200, -160]^\top \ . \tag{25}$$

Fig. 4 and Fig. 5 show the effect of the injected measurement bias on the expected value of the steered clocks and consequently on the desynchronization.

IV. Synchronization of Satellite Constellations

In this section we apply the analyses to a constellation of satellites interconnected via OISLs. A schematic representation of the constellation is depicted in Fig. 6: 24 medium Earth orbit (MEO) satellites are distributed on 3 orbital planes and an additional layer of 6 low Earth orbit (LEO) satellites carrying optical clocks in assumed. This scheme reproduces the layout of DLR's proposal for a future GNSS (Kepler) [3]. For the following synchronization analyses we consider two scenarios:

1) MEO+LEO (ML) for optimal performance: each satellite carries an ultra-stable oscillator (USO). The LEO satellites additionally fly an optical iodine clock. All clocks are included in the ensemble;
2) MEO only (Mo) for faster development and deployment: this scenario forgoes the LEO optical clocks and generates the system time uniquely with the MEO clocks.

Each MEO satellite is connected via OISLs to the satellite ahead and to the satellite behind, thus forming 3 orbital rings.

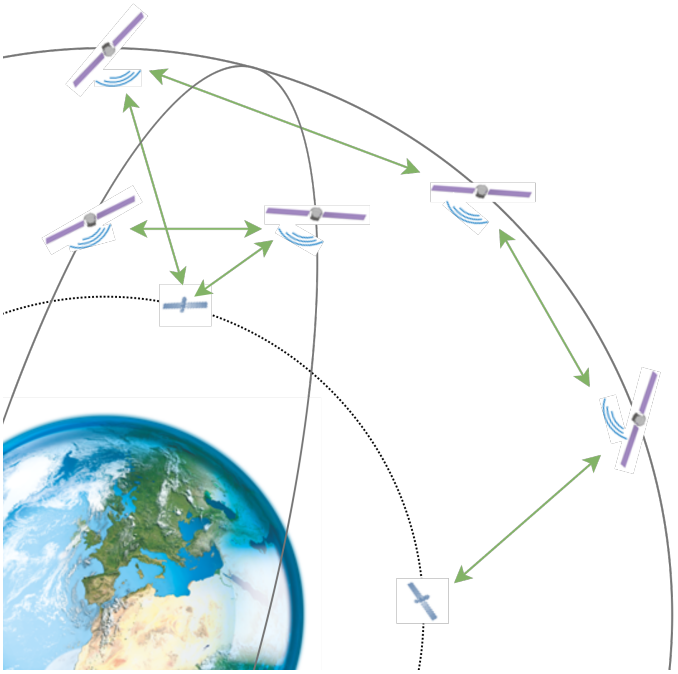

Fig. 6. Conceptual scheme of the simulated constellation: 24 MEO navigation satellites on 3 orbital planes are interconnected with OISLs. 6 additional LEO satellites provide interplanar connection via OISLs.

TABLE I
CLOCK MODEL PARAMETERS USED IN THE SIMULATIONS

Clock	$q_x\,[\mathbf{s}]$	$q_y\,[\mathbf{s}^{-1}]$	**Gauss-Markov processes**	
			$U\,[\mathbf{s}]$	$R\,[\mathbf{s}^{-1}]$
USO	$5.98 \cdot 10^{-26}$	$1.80 \cdot 10^{-29}$	$7.97 \cdot 10^{-27}$	0.0157
			$1.56 \cdot 10^{-26}$	$1.89 \cdot 10^{-3}$
Optical	$3.57 \cdot 10^{-29}$	$3.64 \cdot 10^{-33}$	$1.07 \cdot 10^{-29}$	0.157
			$5.52 \cdot 10^{-30}$	0.013
			$7.70 \cdot 10^{-30}$	$1.6 \cdot 10^{-3}$

Each LEO satellite connects to 3 different MEO satellites, one on each orbital ring. The topology is kept constant during the simulation. The clock model parameters used in the simulations are listed in Table I.

A. Nominal performances

In the nominal scenario, we simulate the measurement noise in two cases: in the best case the measurement noise variance on the OISLs is set to 10^{-25} (corresponding to 0.3 ps/0.1 mm) according to the results shown in [10], while in the worst case it is increased to 10^{-23} (corresponding to 3 ps/1 mm). The onboard measurement noise on LEO satellites is set to 10^{-30} (1 fs). No measurement bias is present. The clocks are randomly initialized in the range 0.5 ± 1 ps and steered every second. The resulting synchronization levels are shown in Fig. 7: as expected, the full constellation shows better synchronization levels than MEO only, and the measurement noise covariance directly impacts the desynchronization. The synchronization levels are reported in Table II: in the case with low measurement noise, both scenarios reach a 2 ps synchronization level for more than 99% of the times.

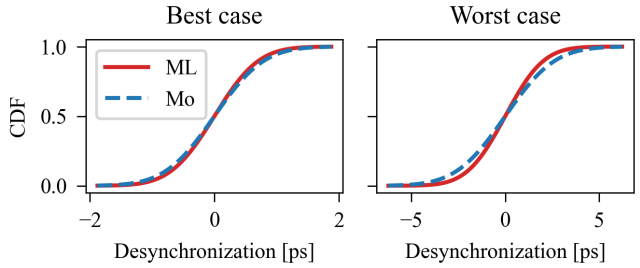

Fig. 7. Cumulative distribution function (CDF) of the maximum desynchronization between clocks in the nominal scenario for MEO+LEO (ML) and MEO only (Mo), with low and high measurement noise covariance.

TABLE II
NOMINAL SYNCHRONIZATION LEVELS

Scenario	**Best case**	**Worst case**
MEO+LEO	99.97% < 2 ps	93.88% < 3 ps, 99.81% < 5 ps
MEO only	99.85% < 2 ps	85.25% < 3 ps, 98.42% < 5 ps

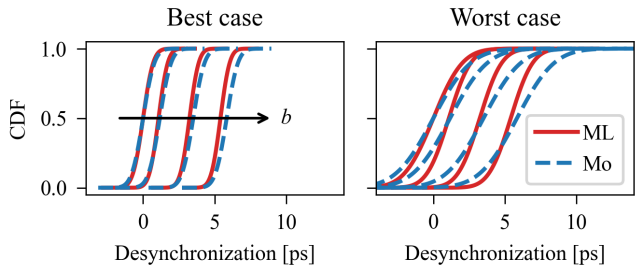

Fig. 8. Cumulative distribution function (CDF) of the maximum desynchronization between clocks for MEO+LEO (ML) and MEO only (Mo), in the presence of increasing measurement bias, and with low or high measurement noise covariance. The arrow indicates increasing magnitude of the injected bias.

B. Non-nominal performance: constant measurement biases

In this case, a constant bias is injected to each OISL. Its value is drawn from a uniform distribution between zero and an increasing maximum magnitude:

$$\mathbf{b} = b\boldsymbol{\mu},\ b \in \{1\text{ ps},\ 3\text{ ps},\ 5\text{ ps}\},\ \mu_i = \mathcal{U}[0,1] \qquad (26)$$

The resulting distributions of the maximum desynchronization can be seen in Fig. 8, and the synchronization levels in Table III. A measurement bias directly impacts the achievable synchronization level of the constellation, with almost a one-to-one mapping between the bias magnitude and the mean value of the distribution of the desynchronization. Thanks to the additional number of clocks and to the presence of the optical clocks, the full constellation is slightly less sensitive to the presence of such a bias.

TABLE III
SYNCHRONIZATION LEVELS IN PRESENCE OF MEASUREMENT BIAS

Scenario	**Best case**		
	Bias - 1 ps	***Bias - 3 ps***	***Bias - 5 ps***
MEO+LEO	96.48% < 2 ps	99.97% < 5 ps	99.92% < 7 ps
MEO only	90.87% < 2 ps	99.17% < 5 ps	96.85% < 7 ps
	Worst case		
	Bias - 1 ps	***Bias - 3 ps***	***Bias - 5 ps***
MEO+LEO	99.94% < 5 ps	99.90% < 7 ps	99.99% < 10 ps
MEO only	96.88% < 5 ps	95.55% < 7 ps	97.84% < 10 ps

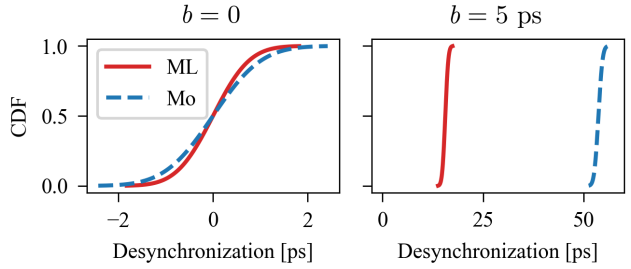

Fig. 9. Cumulative distribution function (CDF) of the maximum desynchronization between clocks for MEO+LEO (ML) and MEO only (Mo), in a open ring configuration, in nominal conditions (left) or in the presence of a 5 ps measurement bias (right).

C. Open and closed ring configuration

An additional simulation has been executed, where the MEO orbital ring of inter-satellite connections has been opened. This reproduces a scenario in which one of the OISLs is unavailable, for instance due to hardware failure, temporary interruption of the optical path, etc. We call such a case *open ring* configuration, compared to *closed ring*, where all the OISLs are established and available.

The resulting synchronization levels in the open ring configuration are shown in Fig. 9: the left plot shows the performance of the two constellation in nominal conditions (no measurement bias), while in the right plot are the synchronization levels achieved in presence of a 5 ps bias. If no bias is present, an open ring does not significantly degrade the performance of the synchronization scheme (compare with Fig. 7). However, if a measurement bias is affecting the system, the results are greatly impacted, with synchronization errors several times higher than the injected bias. The OISL closing the ring can be seen as an implicit constraint acting on the system, stating that all differential measurements along a ring must sum to zero. Thus, in a closed ring configuration a measurement bias can be better compensated. Instead, an open ring configuration lacks this constraint, reducing the system's stiffness and resulting in higher desynchronization values. A MEO only constellation, additionally missing the OISLs between LEO and MEO segment is more sensitive to an open ring configuration, showing desynchronization levels of more than 50 ps.

V. CONCLUSIONS

We described a synchronization scheme that can be applied to constellations of satellites interconnected by OISLs. The scheme establishes a distributed in-space clock ensemble consisting of the satellites' clocks, which are compared using OISLs. Each satellite uses a Kalman filter and a feedback loop to steer the local clock to the composite timescale and to generate a copy of the system time. This results in a tight synchronization of the constellation.

The synchronization performance can be estimated by means of recursions, which compute the mean and variance of the desynchronization between the satellites. The recursions have been validated by corresponding Monte-Carlo simulations. We showed that a constellation of satellites interconnected via OISLs can achieve picosecond-level synchronization across all satellites by implementing this synchronization scheme. Furthermore, we showed how unmodelled measurement biases decrease the synchronization of the constellation. The effects of these biases are reduced if the satellites are connected in a closed ring with a redundant OISL.

REFERENCES

[1] ESA. (2015, November) Esa signs contract for new generation of galileo. [Online]. Available: https://www.esa.int/Applications/Navigation/ESA_signs_contract_for_new_generation_of_Galileo

[2] J. Surof, J. Poliak, R. Wolf, L. Macri, R. M. Calvo, L. Blümel, P. N. Dominguez, G. Giorgi, L. Agazzi, J. Furthner, and C. Günther, "Validation of kepler time and frequency transfer on a terrestrial range of 10.45km," in *Proceedings of the 35th International Technical Meeting of the Satellite Division of The Institute of Navigation (ION GNSS+ 2022)*, September 2022, pp. 3662–3670. [Online]. Available: https://elib.dlr.de/191410/

[3] C. Günther, "Kepler - satellite navigation without clocks and ground infrastructure," in *Proceedings of the 31st International Technical Meeting of the Satellite Division of the Institute of Navigation 2018 (ION GNSS+ 2018)*, 2018, pp. 849–856. [Online]. Available: https://doi.org/10.33012/2018.15997

[4] J. A. Davis, C. A. Greenhall, and P. W. Stacey, "A kalman filter clock algorithm for use in the presence of flicker frequency modulation noise," *Metrologia*, vol. 42, no. 1, pp. 1–10, 2005. [Online]. Available: http://iopscience.iop.org/article/10.1088/0026-1394/42/1/001/pdf

[5] C. A. Greenhall, "A kalman filter clock ensemble algorithm that admits measurement noise," *Metrologia*, vol. 43, no. 4, pp. 311–321, 2006. [Online]. Available: http://iopscience.iop.org/article/10.1088/0026-1394/43/4/S19/meta

[6] C. Trainotti, T. D. Schmidt, and J. Furthner, "Simulating the Realization of a Mixed Clock Ensemble," in *2019 Joint Conference of the IEEE International Frequency Control Symposium and European Frequency and Time Forum (EFTF/IFC)*. IEEE, apr 2019.

[7] K. R. J. Brown, "The theory of the GPS composite clock," in *Proceedings of the 4th International Technical Meeting of the Satellite Division of The Institute of Navigation (ION GPS)*, ION. ION, 1991, pp. 223–242, albuquerque, NM, September 1990.

[8] M. Gödel, T. D. Schmidt, and J. Furthner, "Comparison between simulation and hardware realization for different clock steering techniques," *Metrologia*, vol. 56, no. 3, p. 035001, may 2019. [Online]. Available: https://iopscience.iop.org/article/10.1088/1681-7575/ab144d

[9] F. L. Lewis, *Optimal estimation: With an introduction to stochastic control theory*, ser. A Wiley-Interscience Publication. New York, NY: Wiley, 1986.

[10] C. Trainotti, M. Dassié, G. Giorgi, A. Khodabandeh, and C. Günther, "Autonomous satellite system synchronization schemes via optical two-way time transfer and distributed composite clock," in *Proceedings of the 35th International Technical Meeting of the Satellite Division of The Institute of Navigation (ION GNSS+ 2022)*. Denver, Colorado: Institute of Navigation, Sep. 2022, pp. 3646–3661.